If we compare their suggestion with the data in Figure 6, we indeed observe, for $\alpha > 0.93$, the reappearance of a new form of Al^{VI} and the disappearance of Al^{V} (for $\alpha > 0.96$ or $\alpha/(1-\alpha) \geq 24$). Finally, above 900 °C, the ^{29}Si and ^{27}Al spectra are consistent with existence of γ-alumina mixed with ill-defined alumino-silicates, in agreement with Meinhold et al.[5] In the alumino-silicate phase, there would be silicon with two Al^{IV} neighbors (samples 96 and 98, Table II).

In conclusion, this work constitutes an additional proof of the capability of high-resolution solid-state NMR for solving problems related to disordered materials.

Acknowledgment. One of us (J.F.L.) thanks the Graduate School and the Laboratory for Surface Studies at UWM for a postdoctoral fellowship. The authors also wish to thank Dr. J. P. Gilson for drawing their attention to the problem treated in this paper and also for providing the samples. NSF Grant DIR-8719808 and NIH Grant RR 04095, which have partially supported the purchase of the GE500 NMR instrument, are gratefully acknowledged.

Ammonia Binds to the Catalytic Mn of the Oxygen-Evolving Complex of Photosystem II: Evidence by Electron Spin-Echo Envelope Modulation Spectroscopy†

R. David Britt,* Jean-Luc Zimmermann,‡ Kenneth Sauer, and Melvin P. Klein

Contribution from the Laboratory of Chemical Biodynamics, Lawrence Berkeley Laboratory, Berkeley, California 94720. *Received October 4, 1988*

Abstract: The mechanism of ammonia inhibition of photosynthetic oxygen evolution has been examined by the pulsed EPR technique of electron spin-echo envelope modulation (ESEEM), revealing the direct coordination of an ammonia-derived ligand to the catalytic Mn complex during the $S_1 \rightarrow S_2$ transition of the oxygen evolution S-state cycle. ESEEM experiments were performed on the "multiline" Mn EPR signal observed in photosystem II enriched spinach thylakoid membranes which were treated with either $^{14}NH_4Cl$ or $^{15}NH_4Cl$ (100 mM, pH 7.5). $^{15}NH_4Cl$ treatment produced modulation of the electron spin-echo signal which arises from an $I = {}^1/_2$ ^{15}N nucleus with an isotropic hyperfine coupling $A(^{15}N) = 3.22$ MHz. $^{14}NH_4Cl$ treatment produced a different ESEEM pattern resulting from an $I = 1$ ^{14}N nucleus with $A(^{14}N) = 2.29$ MHz, and with electric quadrupole parameters $e^2qQ = 1.61$ MHz and $\eta = 0.59$. The ^{14}N electric quadrupole parameters are interpreted with respect to possible chemical structures for the ligand. An amido (NH_2) bridge between metal ions is proposed as the molecular identity of the ammonia-derived ligand to the catalytic Mn of photosystem II.

Photosynthesis is the process by which plants and certain bacterial species convert photon energy into chemical energy. The resultant chemical energy is used to drive biochemical reactions. Higher plant photosynthesis involves two segregated photosystems. Photosystem I (PSI) acts to reduce water-soluble ferredoxin, and photosystem II (PSII) oxidizes water and produces O_2. The initial light-driven electron transfer event in photosystem II creates an electron-deficient pigment molecule with sufficient potential to perform water oxidation. The PSII water oxidation/oxygen evolution process is cyclic, with intermediate states of the oxygen-evolving complex (OEC) designated S_0 through S_4.[1] Each photooxidation of the primary pigment induces a transition in this S-state cycle. Molecular oxygen is released after four photooxidation events, and the complex resets to the least oxidized state, S_0. Each PSII reaction center contains four Mn atoms.[2] These form a protein-bound Mn complex that is thought to be the catalytic center for oxygen evolution. The structure of this Mn complex has been partially characterized by X-ray spectroscopy[3,4] and EPR.[5-12] Of particular interest is the discovery of a low-temperature "multiline" EPR signal which presents approximately 19 partially resolved hyperfine lines and is associated with the S_2 state of the Kok cycle.[5] The S_2 multiline EPR spectrum is rather similar to EPR spectra observed with di-μ-oxo bridged Mn(III)Mn(IV) dimers,[13] which suggests that the S_2 signal arises from a similar Mn complex. In such a model complex, the electronic spins of the two Mn ions are correlated by strong antiferromagnetic exchange interactions. The ground state has an effective electronic spin $\tilde{S} = {}^1/_2$. The EPR signal resulting from this effective spin is nearly isotropic and centered near $g = 2$. The EPR spectrum is split into 16 well-resolved lines resulting from hyperfine coupling to the two nonequivalent $I = {}^5/_2$ Mn nuclei. The PSII Mn multiline EPR signal results from an analogous exchange-coupled Mn complex, with hyperfine lines resulting from two or more Mn nuclei. Another S_2 EPR signal centered at the $g = 4.1$ region of the spectrum has also been assigned to paramagnetic Mn.[7,8,11,12,14] Analysis of details of EPR

† This is paper 10 in the series The State of Manganese in the Photosynthetic Apparatus.

‡ Present address: Service de Biophysique, Dēpartement de Biologie, Centre d'Etudes Nucléaires de Saclay, 91191 Gif-sur-Yvette Cedex, France.

(1) Kok, B.; Forbush, B.; McGloin, M. *Photochem. Photobiol.* **1970**, *11*, 457-475.
(2) Yocum, C. F.; Yerkes, C. T.; Blankenship, R. E.; Sharp, R. R.; Babcock, G. T. *Proc. Natl. Acad. Sci. U.S.A.* **1981**, *78*, 7507-7511.
(3) Yachandra, V. K.; Guiles, R. D.; McDermott, A.; Britt, R. D.; Dexheimer, S. L.; Sauer, K.; Klein, M. P. *Biochim. Biophys. Acta.* **1986**, *850*, 324-332.
(4) Yachandra, V. K.; Guiles, R. D.; McDermott, A. E.; Cole, J. L.; Britt, R. D.; Dexheimer, S. L.; Sauer, K.; Klein, M. P. *Biochemistry* **1987**, *26*, 5974-5981.
(5) Dismukes, G. C.; Siderer, Y. *Proc. Natl. Acad. Sci. U.S.A.* **1981**, *78*, 274-278.
(6) Hansson, Ö.; Andrēasson, L.-E. *Biochim. Biophys. Acta* **1982**, *679*, 261-268.
(7) Casey, J. L.; Sauer, K. *Biochim. Biophys. Acta* **1984**, *767*, 21-28.
(8) Zimmermann, J. L.; Rutherford, A. W. *Biochim. Biophys. Acta* **1984**, *767*, 160-167.
(9) de Paula, J. C.; Brudvig, G. W. *J. Am. Chem. Soc.* **1985**, *107*, 2643-2648.
(10) de Paula, J. C.; Beck, W. F.; Brudvig, G. W. *J. Am. Chem. Soc.* **1986**, *108*, 4002-4009.
(11) Zimmermann, J. L.; Rutherford, A. W. *Biochemistry* **1986**, *25*, 4609-4615.
(12) Hansson, Ö.; Aasa, R.; Vänngård, T. *Biophys. J.* **1987**, *51*, 825-832.
(13) Cooper, S. R.; Dismukes, G. C.; Klein, M. P.; Calvin, M. *J. Am. Chem. Soc.* **1978**, *100*, 7248-7252.

0002-7863/89/1511-3522$01.50/0

and X-ray spectroscopy results have led to a number of differing suggestions for the specific configuration of the Mn ions in the OEC, including a single Mn tetramer,[10,15,16] a single Mn dimer with one or two proximate Mn monomers,[3,4,12,17] or a pair of Mn dimers.[3,4,18]

Low concentration treatments with certain amines, including NH_3, NH_2CH_3, and Tris (2-amino-2-hydroxymethylpropane-1,3-diol), provide for reversible oxygen evolution inhibition. A possible mechanism for this inhibition involves the amines binding as Lewis bases with respect to the Lewis acid Mn, thereby competing for binding sites with a primary substrate, water. Hind and Whittingham[19] studied the effects of varying both buffer pH and NH_4Cl concentration on the rates of ferricyanide reduction by illuminated chloroplasts and concluded that inhibition of the Hill reaction is caused by the unprotonated ammonia base NH_3. Izawa et al.[20] demonstrated that the inhibition of the Hill reaction by NH_3 occurs by blocking water oxidation. Free-base ammonia concentrations sufficient to inhibit the Hill reaction with only water available as a PSII electron donor had little effect on the Hill reaction rates when NH_2OH was added as an alternate electron donor. Velthuys[21] provided kinetic resolution to the study of ammonia inhibition of oxygen evolution by measuring the effects of ammonia on the flash-induced luminescence of chloroplasts. This study suggested the presence of ammonia binding sites at the S_2 and S_3 states of the Kok S-state cycle. No interaction between ammonia and the OEC was found in the dark-adapted S_1 state. Sandusky and Yocum[22,23] described two independent sites for amine inhibition of oxygen evolution. The type I (SY I) site shows inhibition by a class of amines (ammonia, Tris, methylamine, 2-amino-2-ethylpropanediol, and *tert*-butylamine) which is competitive with respect to Cl^- concentration. The binding strength of each amine was observed to be proportional to the amine pK_α, an observation considered indicative of a metal binding site. A second ammonia inhibition site (SY II) was observed which shows no competitive relationship with Cl^-. This site was accessible to only ammonia. The other amines tested, all physically larger than ammonia, only showed the chloride competitive form of inhibition. Sandusky and Yocum proposed this SY II site to be a physically restricted binding site to Mn which is normally occupied by the native substrate, water. The SY I site was proposed to be another binding site to Mn, but normally occupied by the essential oxygen evolution cofactor, Cl^-.

The nature of amine binding to the OEC has recently been studied by EPR.[24-31] Of particular interest is the observation by Beck et al.[24] of an alteration in the line shape and hyperfine spacings of the Mn multiline EPR signal under conditions corresponding to ammonia inhibition of oxygen evolution at the SY II site. This result showed that ammonia interacts with the OEC at a site which affects the magnetic properties of the Mn cluster that gives rise to the multiline EPR signal. Beck et al. advanced the proposal that the alteration in EPR properties results from direct coordination of one or more NH_3-derived ligands to the PSII Mn. However, they also note the possibility of the altered multiline EPR signal arising from NH_3 binding to a remote site which affects the environment of the Mn ions sufficiently to alter their EPR signature. No significant differences were reported in the altered multiline EPR signal with samples prepared by either $^{14}NH_4Cl$ or $^{15}NH_4Cl$ treatment.[24] Thus there is no direct spectroscopic evidence from EPR to demonstrate direct coordination of the ammonia-derived nitrogen to the Mn complex. In addition, Boussac and Rutherford[32] have demonstrated an alteration in the Mn multiline EPR signal similar to that effected by ammonia treatment by replacement of the essential oxygen evolution cofactor Ca^{2+} with Sr^{2+}. Certainly Sr^{2+} is not binding directly to Mn in a manner analogous to that proposed for NH_3, yet the effect of the multiline EPR signal is similar. This observation further raises the possibility that the EPR signal alteration upon NH_3 treatment arises from a remote binding site also, with remote NH_3 binding and Sr^{2+} replacement of Ca^{2+} inducing a similar conformation of the Mn site, which results in the altered form of the Mn multiline EPR signal. Thus although the observation of an alteration in the form of the multiline EPR signal implies a NH_3 binding site on the OEC which influences the environment of the Mn cluster, it cannot be accepted as definitive evidence of direct NH_3 ligation to the catalytic Mn of the oxygen-evolving complex.

In this paper we report the results of electron spin–echo envelope modulation (ESEEM) experiments undertaken to examine possible ammonia coordination to the catalytic Mn of the PSII OEC. In conventional continuous-wave (CW) EPR, a small fraction of the applied microwave radiation is absorbed by those electron spins in resonance. The incident microwave power is typically kept sufficiently low to avoid saturation of the electron spin populations. The spin system is therefore maintained near thermal equilibrium. Pulsed EPR is performed in a different manner, with powerful microwave pulses effecting large rotations of the net electron spin magnetization on a time scale short compared to the relaxation processes which return the electron spin magnetization to equilibrium. For very narrow EPR signals, the EPR spectrum can be obtained by Fourier analysis of the free induction decay (FID) following a single microwave pulse. However, the large bandwidths of most EPR signals, in particular those associated with transition metals, preclude such simple pulsed EPR experiments. In such cases only a small fraction of an inhomogeneously broadened EPR line is excited by the microwave pulse. The FID may reflect only the excitation profile of the incident pulse and often decays to undetectable power levels before the instrument receiver recovers from the pulses. However, the rapid dephasing due to inhomogeneous broadening may be refocused with multiple pulse sequences, resulting in one or more observable electron spin–echoes. In addition to inducing the electron spin transitions, the microwave pulses may also induce "semiforbidden" transitions of paramagnetic nuclear moments magnetically coupled to the electron spins, resulting in quantum mechanical coherences in the nuclear spin sublevels associated with the electron spin levels. These coherences create interference effects which can be measured by varying the electron spin–echo pulse timings. Fourier analysis of the resulting electron spin–echo envelope modulation pattern reveals the frequencies of the various nuclear transitions.[33-37]

(14) Cole, J.; Yachandra, V. K.; Guiles, R. D.; McDermott, A. E.; Britt, R. D.; Dexheimer, S. L.; Sauer, K.; Klein, M. P. *Biochim. Biophys. Acta* **1987**, *890*, 395–398.
(15) Dismukes, G. C.; Ferris, K.; Watnick, P. *Photobiochem. Photobiophys.* **1982**, *3*, 243–256.
(16) Brudvig, G. W.; Crabtree, R. H. *Proc. Natl. Acad. Sci. U.S.A.* **1986**, *83*, 4586–4588.
(17) Hansson, Ö. Ph.D. Thesis, Department of Physics, Chalmers University of Technology, Göteborg, Sweden, 1986.
(18) Guiles, R. D. Ph.D. Thesis, Department of Chemistry, University of California—Berkeley, Lawrence Berkeley Laboratory Report LBL-25186, 1988.
(19) Hind, G.; Whittingham, C. P. *Biochim. Biophys. Acta* **1963**, *75*, 194–202.
(20) Izawa, S.; Heath, R. L.; Hind, G. *Biochim. Biophys.* **1969**, *180*, 388–398.
(21) Velthuys, B. R. *Biochim. Biophys. Acta* **1975**, *396*, 392–401.
(22) Sandusky, P. O.; Yocum, C. F. *Biochim. Biophys. Acta* **1984**, *766*, 603–611.
(23) Sandusky, P. O.; Yocum, C. F. *Biochim. Biophys. Acta* **1986**, *849*, 85–93.
(24) Beck, W. F.; de Paula, J. C.; Brudvig, G. W. *J. Am. Chem. Soc.* **1986**, *108*, 4018–4022.
(25) Beck, W. F.; Brudvig, G. W. *Biochemistry* **1986**, *25*, 6479–6486.
(26) Beck, W. F.; Brudvig, G. W. In *Progress in Photosynthesis Research*; Biggins, J., Ed.; Nijhoff: Dordrecht, 1987; Vol. 1, pp 499–502.
(27) Aasa, R.; Andrēasson, L.-E.; Lagenfelt, G.; Vänngård, T. *FEBS Lett.* **1987**, *221*, 245–248.
(28) Andrēasson, L.-E.; Hansson, Ö. In *Progress in Photosynthesis* Research; Biggins, J., Ed.; Nijhoff: Dordrecht, 1987; Vol. 1, pp 503–510.
(29) Beck, W. F.; Brudvig, G. W. *J. Am. Chem. Soc.* **1988**, *110*, 1517–1523.
(30) Beck, W. F.; Brudvig, G. W. *Chem. Scr.* **1988**, *28A*, 93–98.
(31) Ono, T.-A.; Inoue, Y. *Arch. Biochem. Biophys.* **1988**, *264*, 82–92.
(32) Boussac, A.; Rutherford, A. W. *Biochemistry* **1988**, *27*, 3476–3483.
(33) Mims, W. B. *Phys. Rev. B.* **1972**, *5*, 2409–2419.
(34) Mims, W. B. *Phys. Rev. B.* **1972**, *6*, 3543–3545.
(35) Mims, W. B. In *Electron Paramagnetic Resonance*; Geschwind, S., Ed.; Plenum Press: New York, 1972; pp 263–351.
(36) Kevan, L. In *Time Domain Electron Spin Resonance*; Kevan, L., Schwartz, R. N., Eds.; Wiley: New York, 1979; pp 279–341.

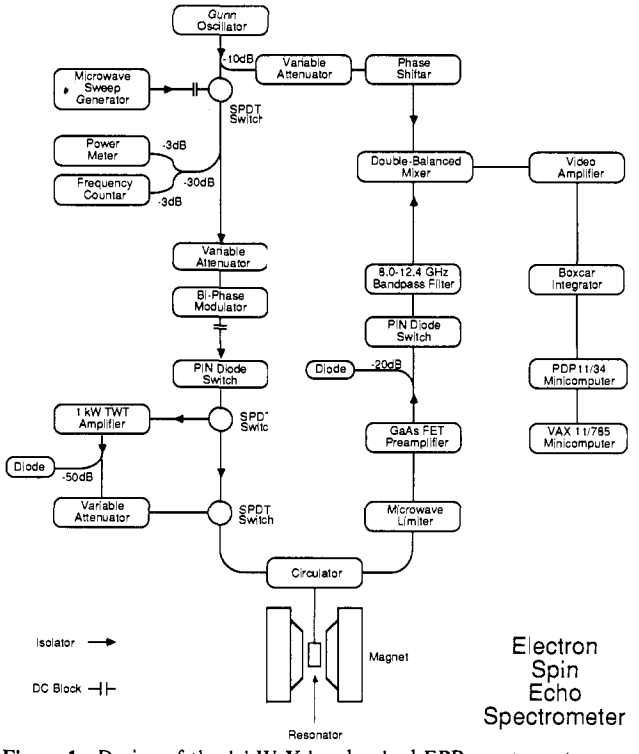

Figure 1. Design of the 1-kW X-band pulsed EPR spectrometer.

We have completed ESEEM experiments on the Mn multiline EPR signal under conditions of ammonia-induced inhibition of oxygen evolution, using either the ^{14}N or ^{15}N nitrogen isotopes of NH_4Cl. The results provide conclusive evidence that an NH_3-derived ligand binds to the Mn complex of the OEC during the $S_1 \rightarrow S_2$ transition. The $^{14}NH_4Cl$-treated samples show new ESEEM frequencies attributable to a single ^{14}N ligand to Mn with an isotropic hyperfine coupling $A(^{14}N) = 2.29$ MHz and electric quadrupole parameters $e^2qQ = 1.61$ MHz and $\eta = 0.59$. The $^{15}NH_4Cl$-treated sample shows a different ESEEM pattern resulting from an ^{15}N ligand to Mn with $A(^{15}N) = 3.22$ MHz, a value proportional to the ^{14}N hyperfine coupling constant by the ratio of the two nuclear moments. Analysis of the electric quadrupole parameters suggests that the ammonia-derived ligand is present as an amido (NH_2) bridge.

Experimental Section

Materials and Methods. O_2-evolving PSII membranes (500 μmol of O_2/mg of chlorophyll (Chl)/h) were prepared by the method of Berthold et al.[38] The PSII membrane pellets were resuspended to a concentration of 2 mg of Chl/mL in a medium containing 0.4 M sucrose, 50 mM NaCl, and 40 mM HEPES (*N*-2-hydroxyethylpiperazine-*N'*-2-ethanesulfonic acid) at pH 7.5 and centrifuged for 15 min at 35000*g*. The resulting pellets were resuspended in a buffer containing 0.4 M sucrose, 5 mM NaCl, and 40 mM HEPES at pH 7.5 and again centrifuged for 15 min at 35000*g*. The resulting pellet was kept in the dark for 15 min to poise the PSII membranes in the dark-stable S_1 state. To stabilize the S_2 state following illumination and subsequent incubation at 20 °C, the electron acceptor PPBQ (phenyl-*p*-benzoquinone) was added from a 20 mM solution in ethanol to a final concentration of 1 mM.[39,40] For NH_4Cl-treated membranes, either $^{14}NH_4Cl$/NaOH pH 7.5 or $^{15}NH_4Cl$/NaOH pH 7.5 (MSD Isotopes) was added for a final NH_4Cl concentration of 100 mM, with a resulting free-base NH_3 concentration of 2 mM. Membrane preparations were loaded into calibrated 2.7-mm i.d. quartz EPR tubes at a concentration of 10 mg of Chl/mL and frozen in liquid N_2. Both EPR and ESEEM spectra were recorded for these dark-adapted S_1-state samples. The samples were then illuminated for 10 min at a temperature of 195 K in an unsilvered Dewar flask containing a mixture of ethanol and solid CO_2. EPR and ESEEM spectra were recorded for these illuminated S_2-state samples. The samples were then warmed to 20 °C for 30 s and immediately frozen in a solid CO_2/ethanol slurry rapidly followed by immersion in liquid N_2. This "annealing" protocol was performed to allow for any ligand substitution or conformational change that may not occur at the 195 K illumination temperature.[24,28] The EPR and ESEEM spectra were then recorded for these "annealed" samples. This protocol results in two sets of EPR and ESEEM spectra for each sample. The "illuminated" spectra are obtained by subtracting the dark S_1-state data from the data obtained following 195 K illumination. The "annealed" spectra are obtained by similar subtraction of the dark S_1-state data from the data obtained following warming to 20 °C.

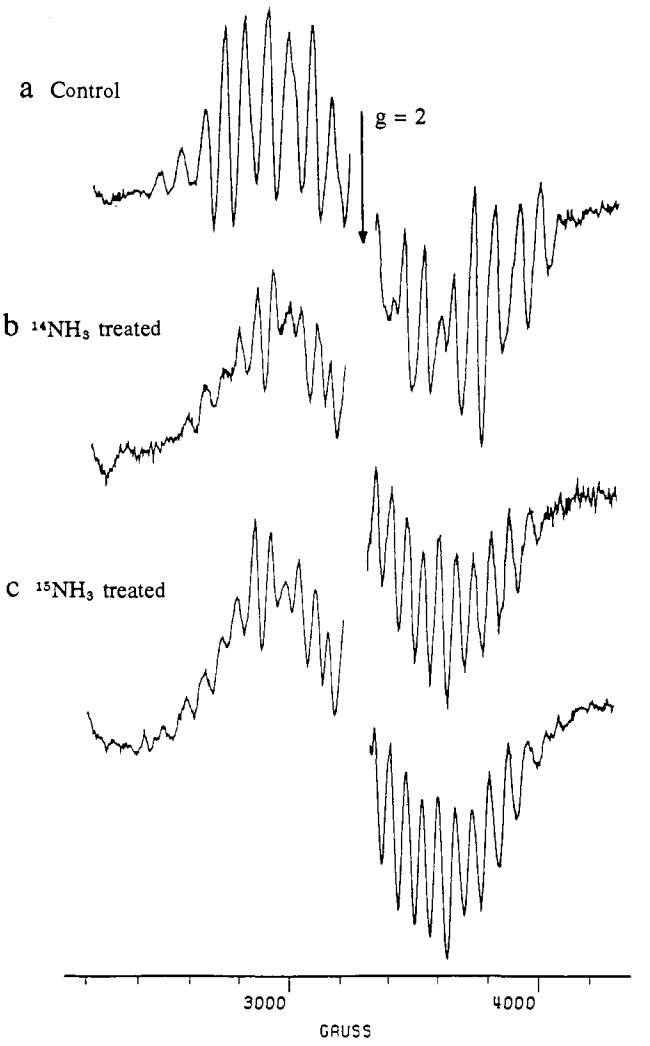

Figure 2. The "annealed" CW EPR spectra obtained for the three samples examined in this work. The control Mn multiline EPR spectrum (a) is obtained with a control pH 7.5 sample with no added NH_4Cl. The "altered" form of the Mn multiline EPR signal is seen following treatment with either $^{14}NH_4Cl$ (b) or $^{15}NH_4Cl$ (c). Both of the NH_4Cl-treated samples reveal the "altered" Mn multiline EPR signal after the annealing process. Dark background spectra are subtracted in all cases.

Spectrometer Design. ESEEM experiments were performed with a home-built pulsed EPR spectrometer. A schematic layout of the pulsed EPR spectrometer is shown in Figure 1. Details of design and operation are provided elsewhere.[41] ESEEM data were obtained with a waveguide-mounted loop-gap resonator probe which allows for rapid introduction of samples into the liquid He bath.[42] All ESE experiments were performed with microwave pulses of 12-ns duration with the applied power set for maximal two- or three-pulse ESE amplitudes (typically 200 W). The two-pulse ESEEM data were taken by gated integration of the ESE signal while varying the interpulse time τ in 10-ns increments over the plotted range. The three-pulse ESEEM patterns were similarly

(37) Mims, W. B.; Peisach, J. In *Biological Magnetic Resonance*; Berliner, L. J.; Reuben, J.; Eds.; Plenum Press: New York, 1981; Vol 3, pp 213–263.
(38) Berthold, D. A.; Babcock, G. T.; Yocum, C. F. *FEBS Lett.* **1981**, *134*, 231–234.
(39) Zimmermann, J.-L.; Rutherford, A. W. *Biochim. Biophys. Acta* **1986**, *851*, 416–423.
(40) Styring, S.; Rutherford, A. W. *Biochemistry* **1987**, *26*, 2401–2405.
(41) Britt, R. D. Ph.D. Thesis, Department of Physics, University of California—Berkely Lawrence Berkeley Laboratory Report LBL-25042, 1988.
(42) Britt, R. D.; Klein, M. P. *J. Magn. Reson.* **1987**, *74*, 535–540.

obtained by incrementing the time T between microwave pulses II and III in 20-ns increments. All ESEEM experiments reported were performed at a temperature of 4.2 K and at a magnetic field value of 3500 G. ESEEM frequency domain results are presented in the form of cosine Fourier transforms, with the short experimental dead times reconstructed with the Fourier backfill technique described by Mims.[43]

Results

EPR and ESE Field-Swept Spectra. Figure 2a displays the "annealed" CW EPR spectrum obtained for a control pH 7.5 sample with no added NH_4Cl. A well-resolved multiline EPR signal attributable to exchange coupled Mn ions is observed under these conditions. The "illuminated" spectrum obtained before warming is similar to this "annealed" spectrum shown in Figure 2a, except for the presence of EPR signals originating from the electron acceptors of PSII (not shown). The "annealed" EPR spectra obtained in samples containing either $^{14}NH_4Cl$ or $^{15}NH_4Cl$ are displayed respectively in Figure 2, b and c. As first reported by Beck et al.,[24] the presence of NH_4Cl induces a modified multiline EPR signal characterized by a larger number of lines and reduced hyperfine spacings. The "illuminated" spectra (not shown) of the samples treated with NH_4Cl are identical with the control spectra, demonstrating that such an annealing step is necessary to trigger the appearance of the modified multiline EPR signal.[24] The "annealed" spectra obtained with either $^{14}NH_4Cl$ or $^{15}NH_4Cl$ are virtually identical,[24] thus providing no direct evidence for attributing the appearance of the modified EPR signal to coordination of a nitrogen ligand to the catalytic Mn.

Figure 3a displays the light-induced ESE spectrum for the control sample. This spectrum is obtained by monitoring the amplitude of the two-pulse electron spin–echo as a function of magnetic field while maintaining a constant interpulse time τ. This ESE spectrum is thus the electron spin–echo–detected analogue of the CW EPR spectrum. The ESE spectrum is not presented as $d\chi''/dH$, the derivative of microwave power absorption with respect to magnetic field, because magnetic field modulation is not employed for noise rejection. However, the ESE spectrum can be numerically differentiated with respect to magnetic field, as displayed in Figure 3b, which clearly shows the Mn multiline spectral pattern. We also note that the shape and linewidth of the light-induced ESE signal is similar to that obtained by integration of the CW multiline EPR spectrum.[12] Hansson et al.[12] have determined that the Mn multiline EPR signal is isotropic with $g = 1.98$. The >1000-G linewidth results solely from the large hyperfine couplings to the Mn nuclei.

We note that subtraction of the dark background spectra is particularly important for the ESE and ESEEM spectra, because broad featureless background lines may be large without the effective high-pass filtering provided by field modulation. The principal background feature appears to be from Cu^{+2}, which may be associated with the LHCII light-harvesting protein.[44]

ESEEM Results. Figure 4 shows the two-pulse ESEEM and corresponding cosine Fourier transform for the "annealed" untreated control sample. There are two prominent features in the frequency domain ESEEM spectrum. The feature at 14.9 MHz results from protons weakly coupled to the electron spin and resonating at or near the proton Larmor frequency.[41] A second large feature is observed at 4.7 MHz. The origin of this feature is discussed in a manuscript in preparation. The "illuminated" ESEEM results obtained before warming the control sample are indistinguishable from these "annealed" results. The two-pulse ESEEM and Fourier cosine transform for the "annealed" $^{15}NH_4Cl$-treated sample are displayed in Figure 5. A new component with a frequency of 3.12 MHz is evident. The "annealed" ESEEM data for the $^{14}NH_4Cl$-treated samples, which are displayed in Figure 6, reveal additional modulation relative to the control at 4.65 MHz (note the scale change of the amplitude axis). The 3.12-MHz feature observed for the $^{15}NH_3$-treated

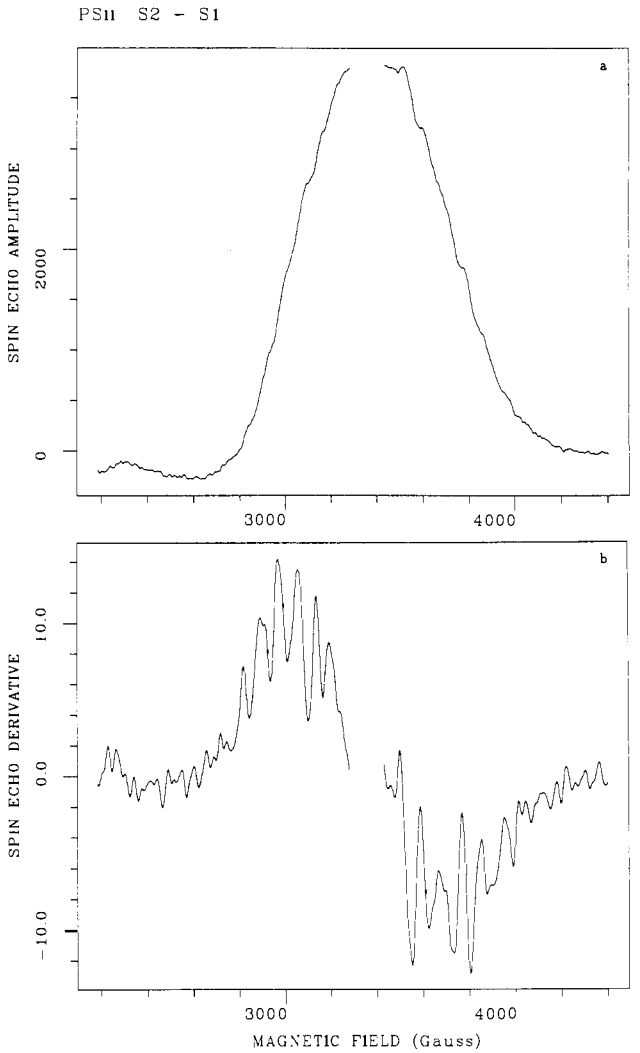

Figure 3. The light-induced Mn EPR signal as observed by electron spin–echo spectroscopy. The spectrum displayed in (a) results from the subtraction of the dark-adapted S_1 spectrum from the illuminated S_2 spectrum. The displayed features are thus all light-induced. The spectra were obtained by measuring the amplitude of a two-pulse electron spin–echo as a function of magnetic field over a 2500-G range centered about 3300 G. The interpulse time τ is 140 ns, and the time interval between successive spin–echo pulse sets is 5.0 ms. The observation temperature is 4.2 K. The microwave frequency is 9.2984 GHz. The derivative of this spectrum with respect to magnetic field is shown in (b) for comparison with conventional field-modulated spectra. The D^+ tyrosine radical signal[45] is excised from the center of both spectra.

sample is not evident in this $^{14}NH_3$-treated sample data. These differences observed for the two nitrogen isotopes of NH_4Cl are conclusive evidence that the observed ESEEM changes result directly from nitrogen nuclei derived from the added NH_4Cl.

There are additional low-frequency transitions observable in the $^{14}NH_4Cl$-treated sample two-pulse ESEEM (Figure 6b). While the relatively short phase memory (800 ns) limits the resolution of these low-frequency features, they are quite clearly resolved in the corresponding three-pulse stimulated echo data displayed in Figure 7, because the three-pulse echo is not subject to phase memory decay.[35-37] Three narrow low-frequency transitions at 0.40, 0.97, and 1.45 MHz are observed in the three-pulse "annealed" ESEEM data for the $^{14}NH_4Cl$-treated sample. These low-frequency peaks are not present in the three-pulse "annealed" ESEEM spectra of either the control or the $^{15}NH_4Cl$-treated samples (data not shown).

Finally we present Figure 8, which shows the ESEEM data for the $^{14}NH_4Cl$-treated sample after illumination but before annealing. These data are similar to the control results, as are the "illuminated" ESEEM data for the $^{15}NH_4Cl$-treated sample (data not shown). The effect of NH_4Cl treatment on the observed

(43) Mims, W. B. *J. Magn. Reson.* **1984**, *59*, 291–306.
(44) Sibbald, P. R.; Green, B. R. *Photosyn. Res.* **1987**, *14*, 201–209.
(45) Barry, B. A.; Babcock, G. T. *Proc. Natl. Acad. Sci. U.S.A.* **1987**, *84*, 7099–7103.

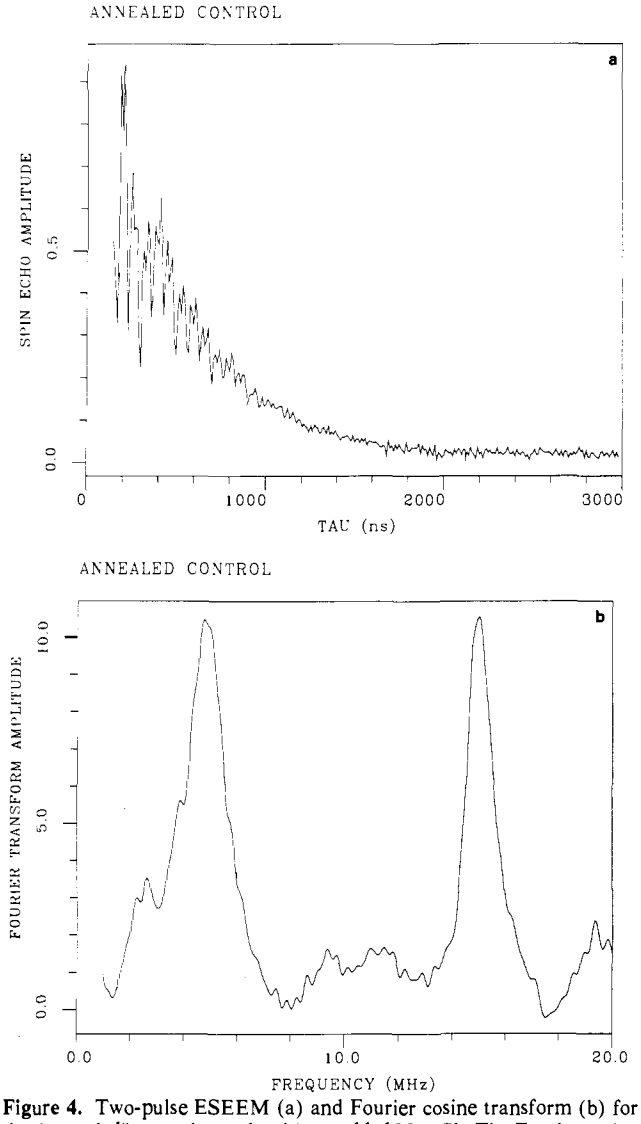

Figure 4. Two-pulse ESEEM (a) and Fourier cosine transform (b) for the "annealed" control sample with no added NH_4Cl. The Fourier cosine transform of the ESEEM pattern is displayed in (b). The spectra were obtained at a temperature of 4.2 K, a microwave frequency of 9.2446 GHz, a magnetic field of 3500 G, and a time interval between spin–echo pulse sets of 4.0 ms.

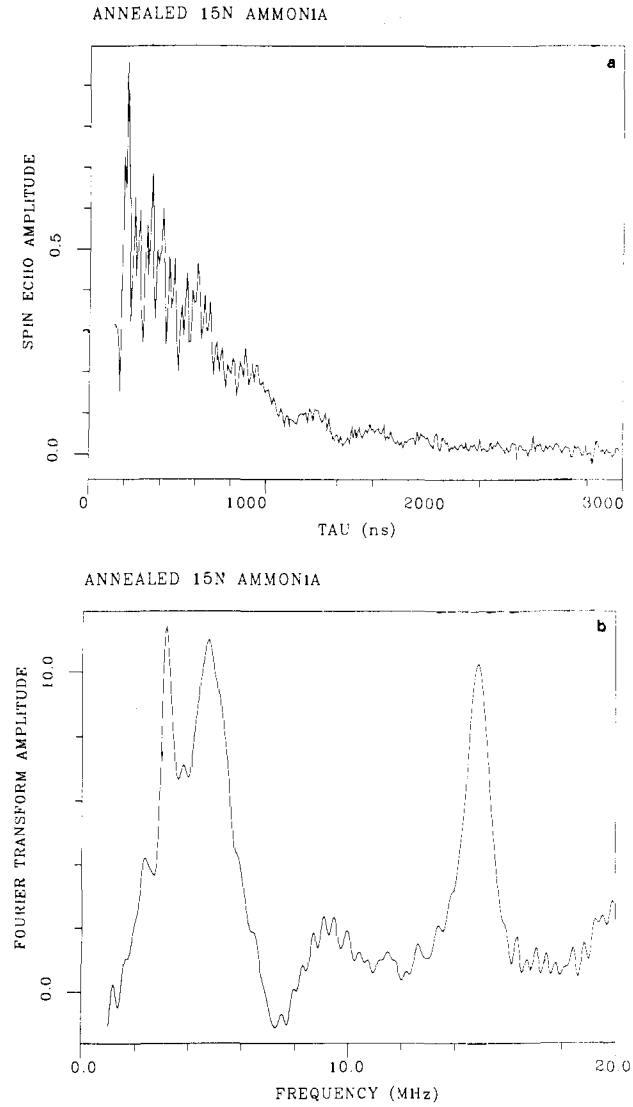

Figure 5. Two-pulse ESEEM (a) and Fourier cosine transform (b) for the "annealed" $^{15}NH_4Cl$-treated sample. The Fourier cosine transform of this ESEEM pattern is displayed in (b). The spectra were obtained at a temperature of 4.2 K, a microwave frequency of 9.2446 GHz, a magnetic field of 3500 G, and a time interval between spin–echo pulse sets of 4.0 ms.

ESEEM patterns thus occurs as a result of the annealing procedure. In this respect the ESEEM changes observed in the NH_4Cl-treated samples upon annealing are correlated with appearance of the "altered" multiline EPR spectra.

ESEEM Analysis. The analysis of the ESEEM pattern of the $^{15}NH_4Cl$-treated sample is simple. The ^{15}N nucleus possesses a nuclear spin $I = {}^1/_2$. The resulting magnetic moment interacts with an effective field resulting from the vector summation of the applied magnetic field and the hyperfine field produced by the electron spin. Each of two $\tilde{S} = {}^1/_2$ electron levels are split into doublet nuclear sublevels. In the simplest analysis, we consider the hyperfine coupling between the nuclear and electron spins to be isotropic and the electron spin to be quantized along the direction of the applied field, resulting in colinear hyperfine and applied magnetic fields. In one of the electronic spin levels, the hyperfine and applied magnetic fields add to produce a larger effective field. We refer to the corresponding sublevel manifold as the β-manifold. The hyperfine and applied fields subtract from one another in the manifold associated with the other electron spin level, and we refer to this as the α-manifold. There are then two $I = {}^1/_2$ nuclear transitions which can be measured by ESEEM:[35-37]

$$\nu_\alpha = \left|\nu_i - \frac{|A|}{2}\right|, \qquad \nu_\beta = \left|\nu_i + \frac{|A|}{2}\right| \tag{1}$$

where ν_i is the nuclear Zeeman frequency due to the external applied field and A is the isotropic hyperfine coupling constant.

The additional peak at 3.12 MHz in the "annealed" ESEEM of the $^{15}NH_4Cl$-treated sample (Figure 5) corresponds to the ν_β transition of eq 1. The ^{15}N Zeeman frequency is $\nu_i = 1.51$ MHz at the observation field of 3500 G. We can then calculate the ^{15}N hyperfine coupling constant to be $A(^{15}N) = 3.22$ MHz. We can scale this value to what is expected for a ^{14}N nucleus, obtaining $A(^{14}N) = 2.29$ MHz. The magnitude of this hyperfine coupling constant is similar to the result $A(^{14}N) = 2.80$ MHz obtained for nitrogen ligands to Mn in exchange-coupled Mn(III)Mn(IV) dimers [di-μ-oxo bridged Mn(III)Mn(IV) with either 2,2′-bipyridine or 1,10-phenantholine ligands].[41] The ν_α transition is not observed in the ESEEM data of Figure 5 because the frequency of this transition is very close to zero ($\nu_\alpha \approx 0.1$ MHz). At the 3500-G field position, the hyperfine field and the applied magnetic field almost completely cancel for the α-manifold.

This cancellation of magnetic field becomes particularly interesting for the $^{14}NH_4Cl$-treated sample ESEEM. The ^{14}N nucleus possesses nuclear spin $I = 1$, with a nonzero electric quadrupole moment. The electric quadrupole moment of the ^{14}N nucleus interacts with electric field gradients at the nucleus to produce nuclear sublevel splittings even in the absence of magnetic field contributions.[46,47] The observed near-cancellation of

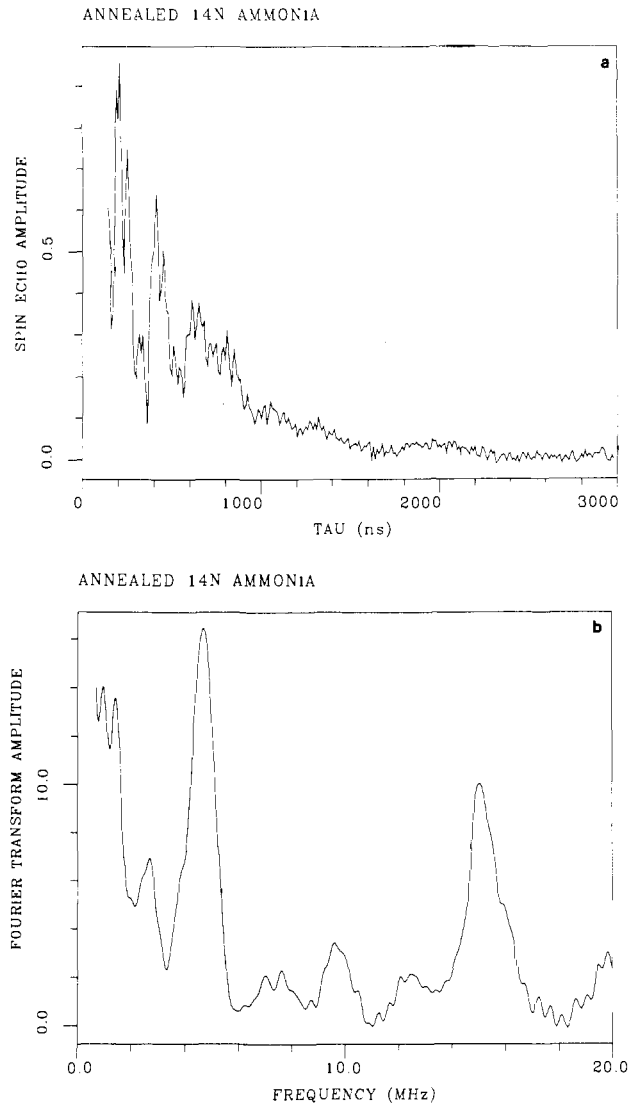

Figure 6. Two-pulse ESEEM (a) and Fourier cosine transform (b) for the "annealed" $^{14}NH_4Cl$-treated sample. The Fourier cosine transform of this ESEEM pattern is displayed in (b). The spectra were obtained at a temperature of 4.2 K, a microwave frequency of 9.2446 GHz, a magnetic field of 3500 G, and a time interval between spin–echo pulse sets of 4.0 ms.

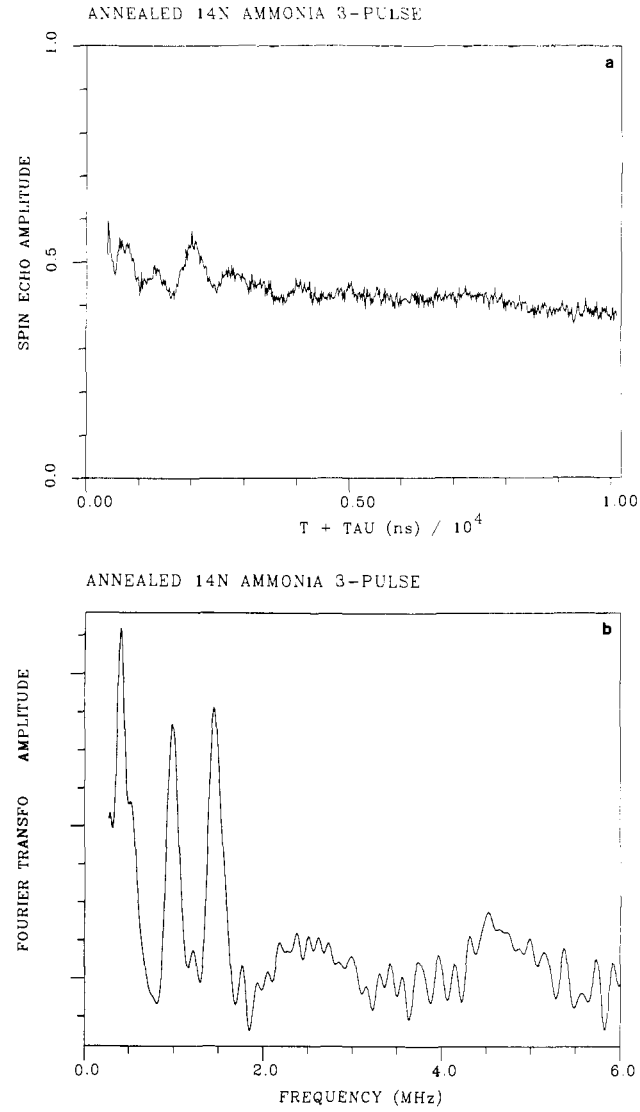

Figure 7. Three-pulse ESEEM (a) and Fourier cosine transform (b) for the "annealed" $^{14}NH_4Cl$-treated sample. The Fourier cosine transform of this ESEEM pattern is displayed in (b). The spectra were obtained at a temperature of 4.2 K, a microwave frequency of 9.2446 GHz, a magnetic field of 3500 G, and a time interval between spin–echo pulse sets of 4.0 ms. The time τ between microwave pulses I and II was set to 200 ns.

magnetic field in the α-manifold results in transitions at frequencies very close to the zero-field nuclear quadrupole resonance (NQR) frequencies[48,49] for the ^{14}N nucleus derived from $^{14}NH_4Cl$ treatment. We assign the low-frequency transitions observed in the three-pulse ESEEM of Figure 7 to these NQR transitions.

The first step in the analysis of the "annealed" ESEEM of the $^{14}NH_4Cl$-treated samples is to discuss the pure electric quadrupole interaction which gives rise to these α-manifold transitions observed in Figure 7. We thus begin with the $I = 1$ ^{14}N nucleus located in a field gradient with principal values $V_{xx} \equiv eq_{xx}$, $V_{yy} \equiv eq_{yy}$, and $V_{zz} \equiv eq_{zz}$. The ordering of the principal axes is chosen such that $|q_{xx}| \leq |q_{yy}| \leq |q_{zz}|$. For the $I = 1$ ^{14}N nucleus, the quadrupolar Hamiltonian $\mathcal{H}_Q$ may be written[50]

$$\mathcal{H}_Q = \frac{e^2qQ}{4}[3I_z^2 - I^2 + \eta(I_x^2 - I_y^2)] \qquad (2)$$

where Q is defined as the scalar quadrupole moment for the ^{14}N nucleus, $q \equiv q_{zz}$, and the asymmetry parameter η is defined by:

$$\eta = \left|\frac{q_{xx} - q_{yy}}{q_{zz}}\right| \qquad (3)$$

The eigenvalues corresponding to this zero-field Hamiltonian are $^1/_4(1 + \eta)e^2qQ$, $^1/_4(1 - \eta)e^2qQ$, and $-^1/_2e^2qQ$. The three corresponding NQR transitions are given by:

$$\nu_+ = \tfrac{1}{4}(3 + \eta)e^2qQ \qquad \nu_- = \tfrac{1}{4}(3 - \eta)e^2qQ$$
$$\nu_0 = \tfrac{1}{2}\eta e^2qQ \qquad (4)$$

We assign the low-frequency transitions observed in the three-pulse "annealed" ESEEM of the $^{14}NH_4Cl$-treated sample to these three NQR transitions as $\nu_+ = 1.45$, $\nu_- = 0.97$, and $\nu_0 = 0.40$ MHz. The experimental frequencies meet the required condition $\nu_+ - \nu_- = \nu_0$ to within the accuracy of the data, and taking the two higher frequencies to be most accurate, we obtain the electric quadrupole parameters $e^2qQ = 1.61$ MHz and $\eta = 0.59$ for the coordinated ^{14}N nucleus.

The additional 4.65-MHz component observed in the two-pulse "annealed" ESEEM of the $^{14}NH_4Cl$-treated sample originates

(46) Das, T. P.; Hahn, E. L. *Solid State Phys.* **1958**, *5*, Suppl. 1, 1-223.
(47) Lucken, E. A. C. *Nuclear Quadrupole Coupling Constants*; Academic Press: London, 1969.
(48) Mims, W. B.; Peisach, J. *J. Chem. Phys.* **1978**, *69*, 4921–4930.
(49) Flanagan, H. L.; Singel, D. J. *J. Chem. Phys.* **1987**, *87*, 5606–5616.
(50) Casabella, P. A.; Bray, P. J. *J. Chem. Phys.* **1958**, *28*, 1182–1187.

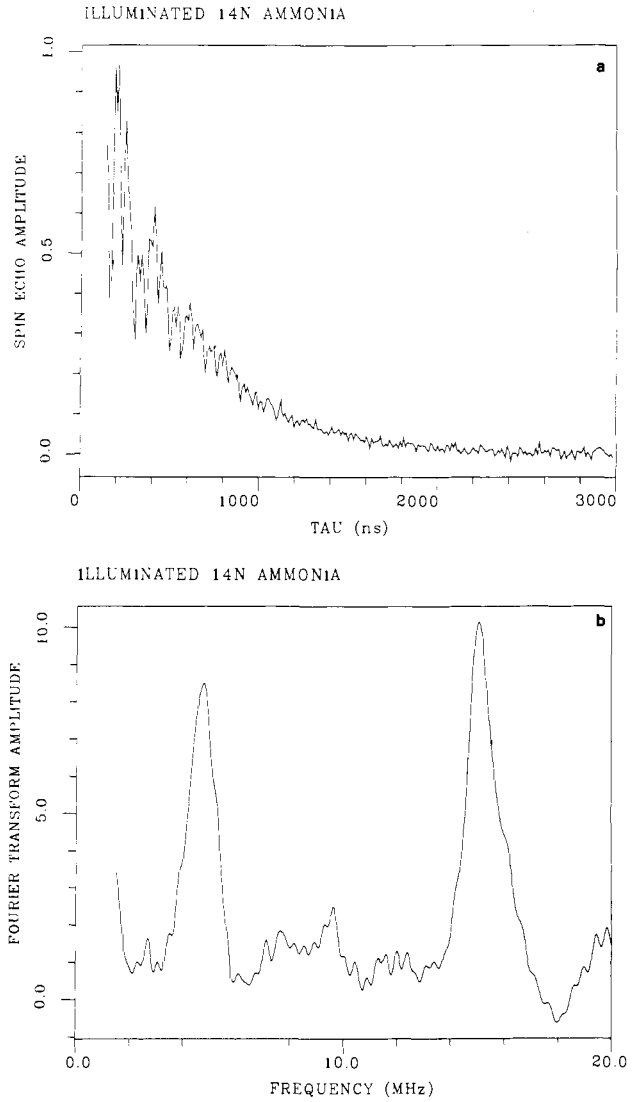

Figure 8. Two-pulse ESEEM (a) and Fourier cosine transform (b) for the "illuminated" $^{14}NH_3$-treated sample. The Fourier cosine transform of this ESEEM pattern is displayed in (b). The spectra were obtained at a temperature of 4.2 K, a microwave frequency of 9.2446 GHz, a magnetic field of 3500 G, and a time interval between spin-echo pulse sets of 4.0 ms.

from the β-manifold, in which the hyperfine and externally applied fields add. To examine the origin of this spin feature, we must include both the electric quadrupole and magnetic dipole terms to the spin Hamiltonian. To this end we supplement the Hamiltonian of eq 2 by adding the effect of a magnetic field vector of frequency-normalized magnitude ν_{ef} oriented with spherical angles θ and φ relative to the quadrupolar principal axes. In our analysis of the observed β-manifold frequency we will specify $\nu_{ef} = |\nu_i + {}^1/_2|A||$. The resulting Hamiltonian can be written in matrix form:[50,51]

$$\mathcal{H} = \begin{pmatrix} \frac{e^2qQ}{4}(1+\eta) & \nu_{ef}\sin\theta\cos\varphi & \nu_{ef}\cos\theta \\ \nu_{ef}\sin\theta\cos\varphi & -e^2qQ/2 & -i\nu_{ef}\sin\theta\sin\varphi \\ \nu_{ef}\cos\theta & i\nu_{ef}\sin\theta\sin\varphi & \frac{e^2qQ}{4}(1-\eta) \end{pmatrix} \quad (5)$$

The energy level splittings for a $I = 1$ ^{14}N nucleus in an arbitrary field can be calculated by numerical diagonalization of this spin Hamiltonian. Figure 9 displays the splitting of the energy levels as a function of the effective field ν_{ef} for a given orientation of the field relative to the quadrupole principal axes ($e^2qQ = 1.6$ MHz, $\eta = 0.6$, $\theta = \pi/4$, and $\phi = \pi/4$). The pure NQR frequencies ν_+, ν_-, and ν_0 are observed at $\nu_{ef} = 0$ MHz. The divergence of these levels with increased effective field depends on the spherical angles θ and ϕ. There are three transitions between the three levels. However, unless $\nu_{ef} \gg e^2qQ$ or $\nu_{ef} \ll e^2qQ$, the inner transitions are very anisotropic, and are typically unresolved in the "powder pattern" which results for noncrystalline samples.[41,48,49] However, the so-called "double-quantum" transition, ν_{dq}, between the outer levels remains sharp in the powder pattern averge, and it is this feature which we observe at 4.65 MHz in the two-pulse "annealed" ESEEM for the $^{14}NH_4Cl$-treated sample.

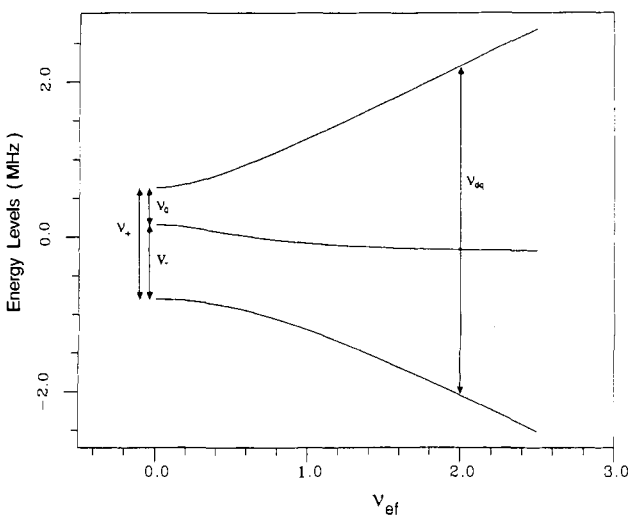

Figure 9. Energy level splittings for a ^{14}N nucleus in an applied magnetic field H_n. These energy levels are obtained by diagonalization of the Hamiltonian expressed in eq 5 as a function of the effective frequency ν_{ef}. The parameters $e^2qQ = 1.6$ MHz, $\eta = 0.6$, $\theta = \pi/4$, and $\phi = \pi/4$ are held fixed. Under conditions of exact cancellation of Zeeman and hyperfine field, the pure NQR frequencies ν_+, ν_-, and ν_0 are observed in the ESEEM spectrum. The contribution from the sublevel manifold where the Zeeman and hyperfine fields add is the "double-quantum" frequency ν_{dq}.

A graphical solution to the Hamiltonian of eq 5 can be used to derive an approximate expression for the double-quantum frequency:[49,52]

$$\nu_{dq} = 2\left[(\nu_i + {}^1/_2|A|)^2 + \frac{(e^2qQ)^2}{16}(3+\eta^2)\right]^{1/2} \quad (6)$$

This expression can be solved for the isotropic hyperfine coupling constant $A(^{14}N)$, given the experimental measurements $e^2qQ = 1.61$ MHz, $\eta = 0.59$, $\nu_{dq} = 4.65$ MHz, and $\nu_i = 1.07$ MHz, resulting in $A(^{14}N) = 2.29$ MHz. This is the same value obtained by scaling the ^{15}N results by the ratio of the $^{14}N/^{15}N$ magnetic moments. We therefore see that the spin-Hamiltonian parameters obtained for the two different nitrogen isotopes are completely consistent in this analysis. The interpretation is also supported by ESEEM results at other field positions throughout the Mn multiline ESE spectrum (data not shown).

So far we have discussed the ESEEM frequencies, but not the ESEEM amplitudes. The ESEEM frequencies observed following either $^{14}NH_4Cl$ or $^{15}NH_4Cl$ treatment can be consistently modeled by a single class of coordinated nitrogen nuclei. There is no spectral evidence for modulation from a second class of nitrogen nuclei. However, it is important to address the question of whether multiple NH_3-derived ligands are bound in one equivalent site. This question can effectively be addressed by comparing theoretical simulations of the ESEEM amplitudes with the experimental data. We can numerically evaluate the ESEEM amplitudes for the $I = 1$ ^{14}N nucleus with the density matrix protocol described by Mims.[33,34] We define as M_α and M_β the 3×3 unitary matrices

(51) Muha, G. M. *J. Chem. Phys.* **1980**, *73*, 4139–4140.

(52) Astashkin, A. V.; Dikanov, S. A.; Tsvetkov, Y. D. *J. Struct. Chem.* **1984**, *25*, 45–55.

which diagonalize the appropriate Hamiltonian for the α- and β-manifolds. The ESEEM amplitudes are encoded in the elements of the unitary matrix $M = M_\alpha^\dagger M_\beta$ which describes the coupling between the α- and β-manifolds induced by the microwave pulses. We perform three-pulse ESEEM experiments by varying the time T between pulses II and III while maintaining the time τ between pulses I and II at a fixed value. Mims derived an expression for the ESEEM pattern for such a three-pulse experiment:

$$E_{\mathrm{mod}}(\tau,T) = \chi_0 + \frac{1}{2}\sum_{i,j}^{i\neq j}{}'\chi_{ij}^{\alpha}[\cos\omega_{ij}^{\alpha}\tau] + \frac{1}{2}\sum_{k,n}^{k\neq n}{}'\chi_{kn}^{\beta}[\cos\omega_{kn}^{\beta}\tau] + \sum_{i,j}^{i\neq j}{}'[\cos\omega_{ij}^{\alpha}(T+\tau)]\left[\frac{1}{2}\chi_{ij}^{\alpha} + \sum_{k,n}^{k\neq n}{}'\chi_{ij,kn}^{\alpha\beta}[\cos\omega_{kn}^{\beta}\tau]\right] + \sum_{k,n}^{k\neq n}{}'[\cos\omega_{kn}^{\beta}(T+\tau)]\left[\frac{1}{2}\chi_{kn}^{\beta} + \sum_{i,j}^{i\neq j}{}'\chi_{ij,kn}^{\alpha\beta}[\cos\omega_{ij}^{\alpha}\tau]\right] \quad (7)$$

In this expression, primed summations indicated that pairs of indices are included in only one order, and the amplitude factors are expressed in terms of the M matrix as

$$\chi_0 = \frac{1}{2I+1}\sum_{i,k}|M_{ik}|^4 \qquad \chi_{ij}^{\alpha} = \frac{2}{2I+1}\sum_{k}|M_{ik}|^2|M_{jk}|^2$$
$$\chi_{kn}^{\beta} = \frac{2}{2I+1}\sum_{i}|M_{ik}|^2|M_{in}|^2 \quad (8)$$
$$\chi_{ij,kn}^{\alpha,\beta} = \frac{2}{2I+1}\mathrm{Re}[M_{ik}^{*}M_{in}M_{jn}^{*}M_{jk}]$$

We see from eq 7 that the three-pulse ESEEM consists of a dc term, plus terms that contain the sublevel interval frequencies in the two manifolds with the conjugate time variable $(T+\tau)$. The amplitudes are observed to be dependent on the fixed time τ.

We can employ eq 7 and 8 to simulate the three-pulse ESEEM pattern of the "annealed" $^{14}NH_4Cl$-treated sample. Our ESEEM studies are performed on nonoriented PSII membranes fragments. The multiline EPR signal for untreated samples is isotropic with $g = 1.98$.[12] The g tensor for the ammonia-altered form of the signal is less well characterized. However, at the magnetic field value used in our X-band experiments, the large Mn hyperfine interactions provide the principal contribution to the total EPR line shape. The ESEEM pattern obtained at a given field position therefore results as a "powder pattern" average of all orientations. In our ESEEM simulations we construct such a "powder pattern" average by summing the individual time domain ESEEM patterns obtained at equal increments of the two independent angular parameters cos θ and ϕ. In these simulations we include an anisotropic component to the nitrogen hyperfine coupling. It is interesting that the ^{15}N ESEEM transition in Figure 5 is so sharp in the presence of nonzero hyperfine anisotropy. The lack of apparent broadening for the $I = {}^1/_2$ ^{15}N nucleus is due to the ESEEM amplitudes being weighted toward certain angles and not reproducing the perfect "powder-pattern ENDOR" spectrum.[53-55] Therefore, these results obtained at only one field position do not provide a quantitative measure of the nitrogen hyperfine anisotropy. In our simulations we assume a simple form for the hyperfine anisotropy by adding an additional axially symmetric hyperfine component with amplitude A_{aniso}. In the limit of a simple dipole–dipole magnetic coupling between the electron and nuclear spins we can express this amplitude as $A_{\mathrm{aniso}} = gg_I\beta\beta_I/hr^3$. The anisotropic amplitude is optimized to provide the best simulation to the experimental data. The result of such a simulation for the three-pulse ^{14}N ESEEM pattern is shown in Figure 10, with simulation parameters $A_{\mathrm{iso}} = 2.29$ MHz, $A_{\mathrm{aniso}} = 0.2$ MHz, $\nu_{\mathrm{I}} = 1.07$ MHz, $e^2qQ = 1.61$ MHz, $\eta = 0.59$, and

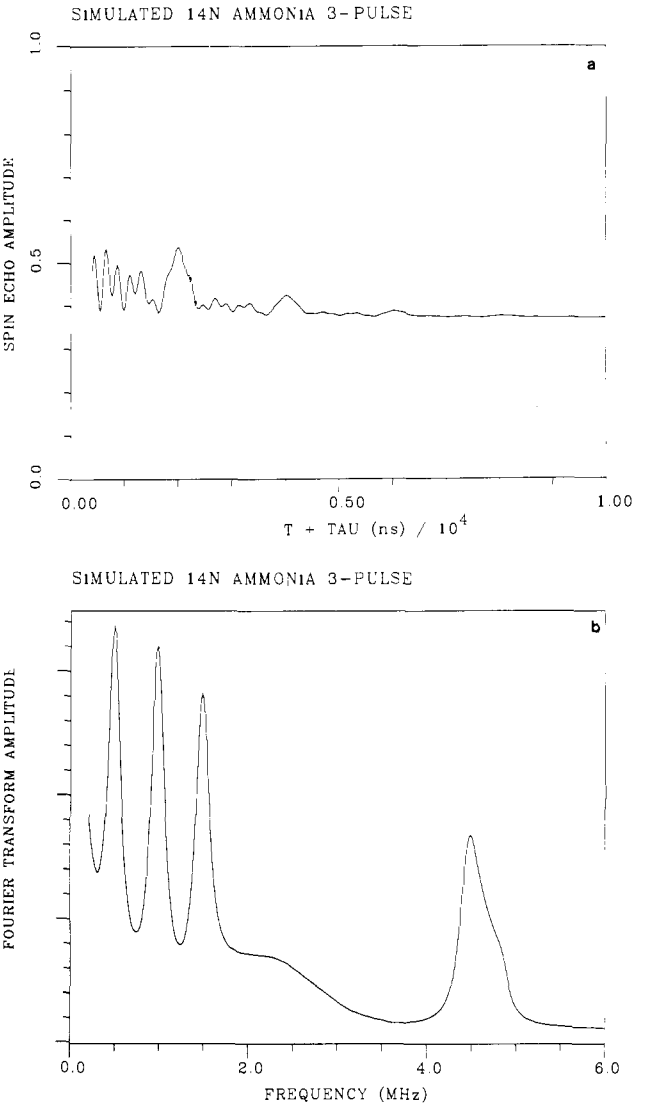

Figure 10. Simulated three-pulse ^{14}N ESEEM for the ammonia-derived Mn ligand. The time-domain simulation is displayed in (a), and the cosine Fourier transform is displayed in (b). The simulation parameters are $A_{\mathrm{iso}} = 2.29$ MHz, $A_{\mathrm{aniso}} = 0.2$ MHz, $\nu_{\mathrm{I}} = 1.07$ MHz, $e^2qQ = 1.61$ MHz, $\eta = 0.59$, and $\tau = 200$ ns. An exponential damping function with a time constant of 2.0 μs is applied to the modulated component of the time-domain data. The simulations result as the sum of 1600 individual time-domain ESEEM patterns obtained by varying in 40 equally spaced increments the independent angular functions cos θ ($0 \rightarrow 1$) and ϕ ($0 \rightarrow \pi/2$).

$\tau = 200$ ns. Exponential damping with a time constant of 2.0 μs is applied to the modulated component of the time domain data of Figure 10a. The corresponding cosine Fourier transform is shown in Figure 10b. The simulated Fourier transform shows the frequency components previously described. The three "pure" NQR transitions are evident, as is the β-manifold "double-quantum" transition at 4.6 MHz. The two inner β-manifold transitions form the very broad shoulder between 2 and 3 MHz.

The time and frequency domain simulated data of Figure 10 may be compared with the experimental three-pulse ESEEM data of Figure 7. The ESEEM simulation for a single coordinated ^{14}N nucleus provides an adequate fit to the experimental data. The amplitudes of the low-frequency modulation components arising from the pure NQR transitions are very similar in the simulated and experimental data, implying that only one NH_3-derived ^{14}N nucleus is present. We also note that the ESEEM pattern arising from multiple nuclei is equal to the product of the individual modulation patterns.[33] For complexes with multiple equivalent nitrogen nuclei, this effect introduces secondary frequencies which are combinations of the individual ^{14}N zero-field frequencies. This

(53) de Groot, A.; Hoff, A. J.; de Beer, R.; Scheer, H. *Chem. Phys. Lett.* **1985**, *113*, 286–290.
(54) Hoff, A. J.; de Groot, A.; Dikanov, S. A.; Astashkin, A. V.; Tsvetkov, Y. D. *Chem. Phys. Lett.* **1985**, *118*, 40–47.
(55) Lai, A.; Flanagan, H. L.; Singel, D. J. *J. Chem. Phys.* **1988**, *89*, 7161–7166.

can be effectively exploited to determine the number of equivalent ^{14}N nuclei.[56] We see no evidence of such combination lines in the ESEEM pattern obtained with $^{14}NH_4Cl$-treated PSII membranes, and we consider this further evidence that only one NH_3-derived ligand is bound at the S_2 state of the oxygen evolution cycle.

Discussion

The electron spin-echo results demonstrate that a single NH_3-derived ligand is coordinated to the Mn complex which gives rise to the multiline EPR signal. There is no evidence of an NH_3-derived ligand bound before the annealing step. We therefore find no evidence of strong NH_3 binding in the S_1 state. Rather, the NH_3-derived ligand binds as a result of the annealing process, indicating the coordination occurs during the $S_1 \rightarrow S_2$ transition, but cannot proceed at the low 195 K illumination temperature. In this respect we find correlation between the binding of the NH_3-derived ligand and the formation of the "altered" multiline EPR signal.[24,25,28]

We proceed to discuss the measured hyperfine and electric quadrupole coupling parameters. The isotropic hyperfine coupling constant for the NH_3-derived ^{14}N nucleus is $A(^{14}N) = 2.29$ MHz. This value is comparable to the value $A(^{14}N) = 2.8$ MHz measured by ESEEM for terminal ^{14}N ligands in di-μ-oxo bridged Mn(III)Mn(IV) model compounds.[41] The relatively small values for the ligand superhyperfine couplings can be explained by simple electrostatic crystal field theory. We expect the high valence Mn ions to exhibit octahedral ligand coordination. The d^3 Mn(IV) ion exists in the $t_{2g}^3e_g^0$ electronic state. The singly-occupied d_{xz}, d_{xy}, and d_{yz} orbitals project away from the coordinating ligands, so the overlap of the unpaired spin density onto the ligand orbitals will be very small. The high-spin d^4 Mn(III) ion exists in the $t_{2g}^3e_g^1$ electronic state. In this case one of the two e_g orbitals is occupied by an unpaired electron, and this orbital will project onto a set of the coordinated ligands. However, the d^4 Mn(III) ion is subject to a large Jahn-Teller distortion which weakens the overlap of the singly-occupied e_g orbital and the ligand orbitals, again resulting in relatively small superhyperfine coupling. The weak superhyperfine couplings expected for these ions can be contrasted to the strong superhyperfine couplings observed for ions such as square-planar d^9 Cu(II), which has a large overlap between the unpaired spin in the $d_{x^2-y^2}$ orbital and the four square-planar ligands.[57,58]

The lack of observable changes in the CW EPR spectra of samples treated with $^{14}NH_4Cl$ versus $^{15}NH_4Cl$[24] results from the small value of the ligand superhyperfine splittings ($\approx$1 G). These splittings are masked by the large inhomogeneous broadening of the EPR line. Resolved superhyperfine features are not observed in di-μ-oxo bridged Mn(III)Mn(IV) model compounds with eight ^{14}N ligands,[13] even though the intrinsic EPR linewidths are much less than those of the PSII Mn multiline signal. We note that EPR studies of the Mn multiline signal with small field modulation amplitudes have demonstrated the presence of additional structure superimposed upon the major partially resolved Mn hyperfine peaks.[59,60] Following the discussion above, we consider it very unlikely that these features result from ligand superhyperfine couplings, because such features would require couplings on the order of those observed for square-planar Cu(II) ions. Rather, we consider these features to arise from more subtle manifestations of the complex multinuclear Mn hyperfine tensors.

We now turn to a discussion of the electric quadrupolar parameters measured for the NH_3-derived ^{14}N ligand. The molecular origin of experimental ^{14}N NQR parameters can be discussed within the framework of the theory of Townes and Dailey.[61] In this simple model, the electric field gradient described by the parameters e^2qQ and η arises primarily from the valence 2p orbitals. Inner closed shells and s orbitals contribute no electric field gradient. For nitrogen compounds of known structure, the occupation numbers of the molecular orbitals can be related to the occupation numbers of the individual atomic orbitals, which can be used to calculate theoretical values for e^2qQ and η.[47] The chemical identity of the ammonia-derived nitrogen species which is ligated to Mn in S_2 is unknown. However, we can limit the range of possibilities by examining the measured values of e^2qQ and η. We first focus on the value of the asymmetry parameter, η.

As described earlier, the asymmetry parameter provides a measure of the degree of axial field gradient symmetry at the site of a nucleus. If the asymmetry parameter $\eta = 0$, the system demonstrates full axial field gradient symmetry about the axis designated z, with principal values $V_{xx} = V_{yy} = -^1/_2eq$ and $V_{zz} = eq$. The condition where $\eta = 1$ corresponds to the greatest deviation from axial symmetry, such that $V_{xx} = 0$, $V_{yy} = -eq$, and $V_{zz} = eq$. Since ammonia inhibition of oxygen evolution occurs via the free-base NH_3 form, an obvious candidate for the NH_3-derived ligand is simply an NH_3 molecule bound to a Mn ion as a terminal ligand. However, the high value of the measured asymmetry parameter, $\eta = 0.59$, argues against the presence of such an axially symmetric ligand. The NH_3 molecule has C_{3v} symmetry. The electric field gradient for perfect C_{3v} symmetry is axial, with an asymmetry parameter $\eta = 0$. A basis set of four sp^3 hybrid orbitals describes NH_3 and its simple derivatives. For free base NH_3, the lone electron pair occupies one orbital. This lone pair is shared with an electron acceptor in the Lewis-acid Lewis-base description of bond formation. The electric field gradient is expected to remain highly axial after coordination with a hard metal ion such the PSII Mn ions. However, we note that some breakdown of the axial symmetry may occur due to hydrogen bonding effects in solid-state samples. We have therefore carefully examined the literature for NQR measurements of ^{14}N nuclei in NH_3 groups.

Crystalline ammonia maintains rigorous axial symmetry (e^2qQ = 3.16 MHz, $\eta = 0.0$),[62] because the hydrogen bonding pattern in the crystal is axially symmetric. Perfect axial symmetry is also maintained for the amino nitrogen in the boron-nitrogen compound H_3BNH_3 ($e^2qQ = 1.253$ MHz, $\eta = 0.0$).[63] A high degree of axial symmetry is observed in the ammonium salts $(CH_3)N^+H_3\cdot Cl^-$ ($e^2qQ = 0.913$ MHz, $\eta = 0.109$) and $(C_2H_5)N^+H_3\cdot Cl^-$ ($e^2qQ = 0.858$ MHz, $\eta = 0.086$).[64] The ^{14}N NQR frequencies for crystalline $[Co(NH_3)_4CO_3]Br$ have been reported.[65] This study is of particular relevance, because the NH_3 groups are directly ligated to a transition metal. Three distinct nitrogen sites were detected by this NQR study. The two equivalent NH_3 group trans to the bidentate CO_3 ligand show a high degree of axial symmetry ($e^2qQ = 1.506$ MHz, $\eta = 0.050$). One of the cis NH_3 groups also has near-perfect axial symmetry ($e^2qQ = 1.678$ MHz, $\eta = 0.006$). The other cis NH_3 group is in a less axially symmetric site ($e^2qQ = 1.248$ MHz, $\eta = 0.326$). The decrease in axial symmetry is apparently due to asymmetry in strong intermolecular hydrogen bonds to neighboring CO_3 groups in the crystal. However, the resultant value of η is still small compared to that of the NH_3-derived ligand to the PSII Mn complex. The amino acids crystallize in the zwitterionic form $N^+H_3\cdot C(R)H\cdot COO^-$. The most extensive set of NH_3 group NQR values is from studies of crystals of amino acids and related compounds.[64,66-72] These NQR results are tabulated in the NQR

(56) McCracken, J.; Pember, S.; Benkovic, S. J.; Villafranca, J. J.; Miller, R. J.; Peisach, J. *J. Am. Chem. Soc.* **1988**, *110*, 1069-1074.
(57) Maki, A. H.; McGarvey, B. R. *J. Chem. Phys.* **1958**, *29*, 35-38.
(58) Kivelson, D.; Neiman, R. *J. Chem. Phys.* **1961**, *35*, 149-155.
(59) Yachandra, V. K.; Guiles, R. D.; Sauer, K.; Klein, M. P. *Biochim. Biophys. Acta* **1986**, *850*, 333-342.
(60) Nugent, J. H. A. *Biochim. Biophys. Acta* **1987**, *893*, 184-189.
(61) Townes, C. H.; Dailey, B. P. *J. Chem. Phys.* **1949**, *17*, 782-796.
(62) Lehrer, S. S.; O'Konski, C. T. *J. Chem. Phys.* **1965**, *43*, 1941-1949.
(63) Lötz, A.; Voitländer, J. *J. Magn. Reson.* **1982**, *48*, 1-8.
(64) Edmonds, D. T.; Hunt, M. J.; Mackay, A. L. *J. Magn. Reson.* **1973**, *9*, 66-74.
(65) Sasane, A.; Smith, J. A. S. *J. Magn. Reson.* **1978**, *32*, 265-287.
(66) Edmonds, D. T.; Speight, P. A. *Phys. Lett.* **1971**, *34A*, 325-326.
(67) Edmonds, D. T.; Summers, C. P. *J. Magn. Reson.* **1973**, *12*, 134-142.
(68) Hunt, M. J. *J. Magn. Reson.* **1974**, *15*, 113-121.
(69) Hunt, M. J.; Mackay, A. L. *J. Magn. Reson.* **1974**, *15*, 402-414.
(70) Hunt, M. J.; Mackay, A. L. *J. Magn. Reson.* **1976**, *22*, 295-301.

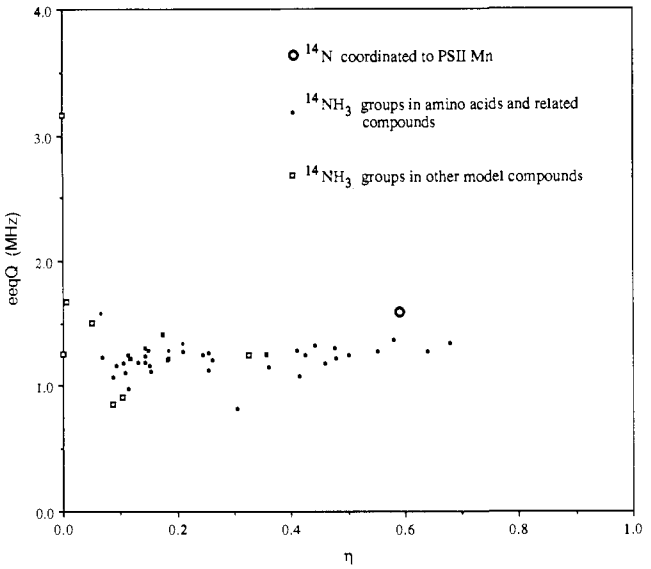

Figure 11. Electric quadrupole coupling parameters e^2qQ and η for the ^{14}N nucleus coordinated to PSII Mn compared with solid-state NQR results for model compounds with NH_3 groups. The ^{14}N NQR parameters for the PSII ammonia-derived Mn ligand are denoted by the open circle (e^2qQ = 1.61 MHz, η = 0.59). Parameters for the NH_3 group models NH_3, H_3BNH_3, $(CH_3)N^+H_3{\cdot}Cl^-$, $(C_2H_5)N^+H_3{\cdot}Cl^-$, and $[Co(NH_3)_4CO_3]Br$ are shown with open boxes. The results for NH_3 groups in amino acids and related compounds are displayed as filled boxes.

review of Edmonds.[73] These results are summarized in Figure 11, which presents the values of e^2qQ and η of 44 different amino acid NH_3 ^{14}N NQR resonance sets (filled squares), along with the previously discussed NH_3 ^{14}N NQR results (open squares), and the values for the NH_3-derived ligand to the PSII Mn complex (open circle). The 44 different amino acid results include multiple resonance sets for some crystal types, different crystal forms for some amino acids, amino acid hydrates and hydrochloride salt crystals, as well as some simple amino acid derivatives.[73] A large degree of scatter is observed in the amino acid NH_3 group asymmetry parameter values. The different values of η arise from differing degrees of breakdown of axial symmetry by hydrogen bonds (both inter- and intramolecular) in the crystals. The average value of η in this group of 44 ^{14}N NQR sets is 0.26. The median value of η is 0.20. The η = 0.59 value for the ^{14}N Mn ligand is much higher than observed for most of these amino acid NH_3 groups. However, we note that a few of the amino acid crystals give values of η greater than 0.5. An example of the effect of hydrogen bond asymmetry on the asymmetry parameter η can be seen in data of glycine crystals. The α-form glycine crystal structure[74] shows near-tetrahedral symmetry for the NH_3 group. However, the electric field gradient symmetry is reduced by the hydrogen bond patterns in the crystal, where two of the nitrogen protons show strong hydrogen bonds to neighboring oxygens, while the third proton shows a weak, bifurcated bond to two further oxygens. A relatively high asymmetry parameter (η = 0.501) results.[64] Another good example of how the local crystal structure affects the asymmetry parameter is observed with crystals of cysteine, which show two distinct NH_3 sites, one with high electric field gradient axial symmetry (η = 0.13), and another site of low axial symmetry (η = 0.64).[67] The differences in the hydrogen bond symmetries of the two sites are apparent in the X-ray crystal structures.[67,75]

The model data discussed above and displayed in Figure 11 are derived from crystalline samples, whereas the ESEEM electric quadrupole data for the ^{14}N ligated to the PSII Mn complex are obtained in a frozen glass. However, the local structure about the ammonia-derived ligand may be well defined on the distance scale of a few angstroms which determines the electric field gradient parameters. We have seen that a few of the amino acid crystals maintain environments with sufficient hydrogen bond asymmetry to cause significant deviation from zero of the asymmetry parameter η for nominally axial NH_3 groups. However, the measured value η = 0.59 for the ammonia derived ligand to Mn is significantly higher than both the average (η = 0.26) and median (η = 0.20) values for crystalline amino acids, and it is much larger than any asymmetry parameter values found in other model systems, including those for NH_3 groups bound to a transition metal. We therefore consider the large asymmetry parameter value for the NH_3-derived ligand to be good evidence for a molecular configuration of lower intrinsic field gradient symmetry than that of an NH_3 group.

Such a reduction of axial symmetry would result from the deprotonation of the NH_3 upon binding to a Mn ion, resulting in a NH_2^- ligand. However, the measured value of e^2qQ for the NH_3-derived ligand appears too be too low for the resultant nitrogen to exist with a residual lone electron pair. ^{14}N compounds with such lone electron pairs typically present $e^2qQ \approx 3$ MHz.[73] We therefore propose that the ligand forms an amido (NH_2) bridge to another metal ion in the Mn OEC cluster. Such amido bridges between metals are common in transition metal inorganic chemistry literature.[76-79] An amido bridge would have an intrinsically large asymmetry parameter in accord with the ESEEM results. The second metal could be another Mn ion of the OEC cluster. An NH_3-derived bridge between Mn ions has been proposed by Beck and Brudvig to explain the formation of the ammonia-altered EPR signal by modulation of the exchange coupling between ions.[26] We also consider the essential oxygen evolution cofactor Ca^{2+} to be a candidate for the second metal ion. Ca^{2+} is involved in the photoactivated reassembly of the Mn complex following disruption by Tris or NH_2OH treatments,[80] and substitution by Sr^{2+} for Ca^{2+} effects an alteration in the Mn EPR signal comparable to that obtained by NH_3 treatment.[32] Thus Ca^{2+} appears to be closely associated with the Mn complex and could serve as the second metal ion associated with a bridging amido group.

Our ESEEM experiments were performed with >100 mM Cl^- in the final buffers. We note that this level of Cl^- is sufficient to shield the Cl^--competitive SY I NH_3 binding site described by Sandusky and Yocum.[22,23] The NH_3-derived Mn ligand observed in our ESEEM experiments should therefore correspond to the SY II NH_3 binding site. This site was also postulated to be a binding site for the native substrate H_2O due to its steric selectivity, because amines larger than NH_3 inhibit oxygen evolution solely at the Cl^--competitive SY I site.[23] Also, treatments with amines bulkier than NH_3 do not trigger the formation of the "altered" multiline EPR signal.[25] Hansson et al. have observed a slight broadening of the Mn hyperfine lines of the multiline EPR signal in samples prepared with $H_2{}^{17}O$ enriched water.[81] This experiment shows that ^{17}O derived from water is accessible to the Mn complex by the S_2 state of the Kok cycle. We have seen from our ESEEM experiments that an NH_3-derived ligand binds to the Mn complex on the $S_1 \rightarrow S_2$ transition. There is no spectroscopic evidence for an NH_3-derived ligand in the less-oxidized S_1 state. We offer a discussion of these observations in the context of the proposed amido bridge. We note that the NH_2^- ion is extremely rare in the aqueous phase (NH_3/NH_2^- has pK_α = 38

(71) Hunt, M. J.; Mackay, A. L.; Edmonds, D. T. *Chem. Phys. Lett.* **1975**, *34*, 473-475.
(72) Edmonds, D. T.; Summers, C. P. *Chem. Phys. Lett.* **1976**, *41*, 482-485.
(73) Edmonds, D. T. *Phys. Rep. C* **1977**, *29*, 233-290.
(74) Jönsson, P.-G.; Kvick, Å. *Acta Crystallogr.* **1972**, *B28*, 1827-1833.
(75) Harding, M. M.; Long, H. A. *Acta Crystallogr.* **1968**, *B24*, 1096-1102.
(76) Chrisoph, G. C.; Marsh, R. E.; Schaefer, W. P. *Inorg. Chem.* **1969**, *8*, 291-297.
(77) Flood, M. T.; Ziolo, R. F.; Earley, J. E.; Gray, H. B. *Inorg. Chem.* **1973**, *12*, 2153-2156.
(78) Kretschmer, M.; Heck, L. *Z. Anorg. Allg. Chem.* **1982**, *490*, 215-229.
(79) Heck, L.; Ardon, M.; Bino, A.; Zapp, J. *J. Am. Chem. Soc.* **1988**, *110*, 2691-2692.
(80) Tamura, N.; Cheniae, G. *Biochem. Biophys. Acta* **1987**, *890*, 179-194.
(81) Hansson, Ö.; Andrēasson, L.-E.; Vänngård, T. *FEBS Lett.* **1986**, *195*, 151-154.

relative to water).[82] The initial interaction of ammonia with the catalytic Mn cluster certainly occurs through the NH_3 form. Upon formation of such a $Mn{\cdot}NH_3$ complex, the pK_α of the NH_3 ligand will be reduced due to the electron affinity of the metal Lewis acid.[83] It is possible that NH_3 forms a transient, weakly bound complex with the Mn cluster in the S_1 state, but only a small fraction of the binding sites are occupied by NH_3 due to competition with 55 M H_2O. The electron affinity of the Mn cluster in the S_1 state is apparently insufficient to effect the NH_3 deprotonation necessary to form the amido bridge. However, the Mn cluster undergoes oxidation during the $S_1 \rightarrow S_2$ transition.[84] This oxidation apparently increases the electron affinity of the cluster sufficiently to trigger deprotonation and metal cation substitution of the NH_3 ligand following binding to the Mn cluster in the S_2 state. The resultant amido bridging ligand is tightly bound and only slowly exchangeable, and water is effectively blocked from reentering the substrate binding site.

(82) Buncel, E.; Menon, B. *J. Organomet. Chem.* **1977**, *141*, 1-7.
(83) Basolo, F.; Pearson, R. G. *Mechanisms of Inorganic Reactions*, 2nd ed.; Wiley; New York, 1967; p 33.
(84) Goodin, D. B.; Yachandra, V. K.; Britt, R. D.; Sauer, K.; Klein, M. P. *Biochim. Biophys. Acta* **1984**, *767*, 209-216.

Conclusions

We have demonstrated via electron spin-echo envelope modulation experiments that a single NH_3-derived ligand binds to the PSII Mn complex during the $S_1 \rightarrow S_2$ transition of the S-state cycle. The NH_3-derived ligand binding appears to be correlated with the formation of the previously described "altered" multiline signal.[24-31] The ESEEM study has determined the magnetic and electric quadrupole coupling parameters for the ^{14}N isotope of nitrogen coordinated to the Mn complex ($A(^{14}N)$ = 2.29 MHz, e^2qQ = 1.61 MHz, and η = 0.59). The hyperfine result is consistent with that measured for the ^{15}N isotope ($A(^{15}N)$ = 3.22 MHz). The electric quadrupole data are interpreted to favor an amido (NH_2) bridge between metal ions as the molecular identity of the NH_3-derived ligand, and a mechanism for the formation of this bridge involving the deprotonation of NH_3 by the Mn cluster in the S_2 state is discussed.

Acknowledgment. This work was supported by the Director, Office of Energy Research, Office of Basic Energy Sciences, Division of Biological Energy of the Department of Energy, under Contract DE-AC03-76SF00098, and by a grant from the U.S. Department of Agriculture (85-CRCR-1-1847). J.-L.Z. is supported by the Commissariat à l'Energie Atomique (France).

Relaxation of the Electronic Spin Moment of Copper(II) Macromolecular Complexes in Solution

Ivano Bertini,*[1a] Claudio Luchinat,[1a,b] Rodney D. Brown, III,[1c] and Seymour H. Koenig[1c]

Contribution from the Department of Chemistry, University of Florence, Via G. Capponi 7, 50121 Florence, Italy, the Institute of Agricultural Chemistry, Faculty of Agricultural Sciences, University of Bologna, Bologna, Italy, and the IBM T. J. Watson Research Center, Yorktown Heights, New York 10598. *Received October 30, 1987*

Abstract: The magnetic field dependence of the longitudinal relaxation rate ($1/T_1$) of solvent protons (NMRD profile) was measured for solutions of Cu^{2+}-substituted transferrin and native (copper-zinc) superoxide dismutase as a function of solvent viscosity, the latter adjusted with sucrose. Similar measurements were made on demetalated transferrin and reduced superoxide dismutase to obtain the diamagnetic background. Both sets of data are found to be dependent on the viscosity of the solvent, as expected. Subtraction of the two sets of data gives the paramagnetic contribution to the NMRD profiles, which is insensitive to solvent viscosity. This indicates that the correlation time for the magnetic interaction of protons with the paramagnetic Cu^{2+} centers is insensitive to thermal (Brownian) rotational motion of the protein. From this it is argued that the longitudinal relaxation time of the electronic spin moment of the Cu^{2+} ions, including the correlation time for its coupling to the thermal motions of the protein, is also insensitive to the rotational thermal motion of the protein. Possible implications for the mechanism of electron relaxation in copper systems in solution are discussed.

Clarification of the mechanisms of magnetic relaxation of the electronic spin moments of paramagnetic metal ions at room temperature, in both small and macromolecular solute complexes, is difficult. ESR, an ostensibly straightforward and direct spectroscopic approach, has many limitations. In particular, measuring the electronic longitudinal relaxation time can be difficult for many reasons: (1) room-temperature ESR spectra may not be detectable either because the electronic relaxation rate is too fast and the lines are too broad or because large zero-field splittings in manifolds with $S > {}^1/_2$ make transitions unobservable at the usual microwave energies; (2) direct measurements of electronic relaxation are restricted, for technical reasons, to the case of very long relaxation times ($\geq 10^{-8}$ s, normally uncommon at room temperature for metal ions); (3) linewidth analyses are often complicated by broadenings unrelated to longitudinal relaxation. An indirect method, however, has been very successful, particularly for Mn^{2+} and Gd^{3+} (S-state ions with half-filled inner shells): inferences about electronic relaxation mechanisms can be drawn from interpretation of the magnetic field dependence of the nuclear magnetic relaxation rate (NMRD—for Nuclear Magnetic Relaxation Dispersion—profile[2]) of solvent protons.[2-5] In such experiments, the NMRD profile of $1/T_1$, the longitudinal

(1) (a) University of Florence. (b) University of Bologna. (c) IBM.

(2) (a) Koenig, S. H.; Schillinger, W. E. *J. Biol. Chem.* **1969**, *244*, 3283. (b) Koenig, S. H.; Schillinger, W. E. *J. Biol. Chem.* **1969**, *244*, 6520.
(3) (a) Koenig, S. H.; Brown, R. D., III; Studebaker, J. *Cold Spring Harbor Symp. Quant. Biol.* **1971**, *36*, 551. (b) Koenig, S. H.; Brown, R. D., III In *ESR and NMR of Paramagnetic Species in Biological and Related Systems*; Bertini, I., Drago, R. S., Eds.; Reidel: Dordrecht, The Netherlands, 1980; p 89.
(4) Bertini, I.; Luchinat, C. *NMR of Paramagnetic Molecules in Biological Systems*; Benjamin Cummings: Menlo Park, CA, 1986.
(5) (a) Koenig, S. H.; Baglin, C.; Brown, R. D., III; Brewer, C. F. *Magn. Reson. Med.* **1984**, *1*, 478. (b) Koenig, S. H.; Brown, R. D., III In *Metal Ions in Biological Systems*; Sigel, H., Ed.; Marcel Dekker: New York, 1986; Vol. 21, p 229. (c) Koenig, S. H.; Epstein, M. *J. Chem. Phys.* **1975**, *63*, 2279.

0002-7863/89/1511-3532$01.50/0